ELSEVIER

Polymer 41 (2000) 2979–2987

polymer

Characterization of ultradrawn polyethylene fibers by NMR: crystallinity, domain sizes and a highly mobile second amorphous phase

W.-G. Hu, K. Schmidt-Rohr*

Department of Polymer Science and Engineering, University of Massachusetts, Amherst, MA 01003, USA

Received 5 March 1999; received in revised form 15 June 1999; accepted 16 June 1999

Abstract

The structure of ultradrawn ultra-high molecular weight polyethylene fibers has been investigated by solid-state NMR. A crystallinity of (88 ± 2)% was determined by traditional ^{1}H NMR lineshape decomposition, and by a new adaptation of ^{13}C NMR crystallinity determination for polyethylenes with extremely long crystalline T_1 relaxation times. ^{1}H spin diffusion yields amorphous domain sizes of 10 ± 5 nm, and crystalline regions of 100 ± 50 nm diameters. A second, highly mobile, amorphous phase, making up (0.8 ± 0.2)% of the sample, was detected by ^{1}H NMR. In spite of its 1.8 kHz ^{1}H line width, it shows little spin diffusion to the other phases, even on a 500-ms time scale; this suggests domains of more than 3 nm thickness or chains extending into voids. Being undetectable in the extruded precursor material and in the fibers after melting, this highly mobile phase must have been induced by the drawing process. ^{13}C NMR confirms that no low-molecular-weight additives are present on a level above 0.01%. A similar highly mobile component has also been detected in drawn medium-molecular-weight polyethylenes. The fraction of partially mobile, oriented interfacial material or tie-molecules in the fiber was found to be ~5%, while rigid *gauche* conformers could not be detected (concentration < 1%). Altogether, five morphological components have been identified: 83% crystal core, of which 80% is orthorhombic and 3% monoclinic, with thickness of ~100 nm; 5% disordered all-*trans* interfacial and/or tie molecules; 11% mobile amorphous regions, with diameters of ~10 nm; and 1% highly mobile segments, probably at void surfaces. On this basis, a structural model for ultradrawn PE fibers is proposed. © 2000 Elsevier Science Ltd. All rights reserved.

Keywords: Polyethylene; Solid-state NMR; Crystallinity

1. Introduction

Ultradrawn, ultraoriented polyethylene fibers (UDF-PE) [1,2] are extremely strong yet lightweight and are used, for instance, in bullet-proof vests. They can be produced by gel spinning [3], or solid-state extrusion and tensile drawing [4–6] of ultra-high molecular weight polyethylene (UHMWPE). Investigation of the morphology is of both fundamental and practical significance, providing an excellent example of a unique microscopic structure that produces outstanding macroscopic properties.

The morphology of UDF-PE has been studied by various techniques. However, even for the crystallinity, the results are not consistent. Transmission electron microscopy (TEM) clearly indicates that lamellar structures are present at small draw ratios but are absent at large draw ratios (>80) [7]. *Gauche* bands in the infrared (IR) spectrum and the peak in small-angle X-ray scattering (SAXS) disappear at draw ratios of >80 [8]. The density [9] and heat content of the amorphous component of the fiber can be different from the bulk material because the chain mobility in the amorphous regions may be different. As a result, crystallinity measurements by IR and SAXS are problematic, and those by differential scanning calorimetry (DSC) and density method have to be used with caution [8]. Crystallinity determination by wide-angle X-ray scattering (WAXS) is also difficult due to the high orientation of the fibers. Traditional ^{13}C direct polarization nuclear magnetic resonance (NMR) cannot give good crystallinity results since the crystalline ^{13}C T_1 relaxation time is extremely long and the amorphous band is broad and low. We will present an approach to make this NMR technique applicable under these difficult circumstances and will compare the results with the crystallinity estimated based on the ^{1}H wideline shape, as well as the results obtained by other techniques in the literature.

Various structural models have been proposed to interpret the unusual morphology and the extraordinary mechanical properties of the fibers [2,10–15]. One of the contentious points is how the amorphous phase is distributed in the fiber. In the "continuous crystal" model [2,11], the amorphous

* Corresponding author. Tel: +1-413-577-1417; fax: +1-413-545-0082.
E-mail address: srohr@polysci.umass.edu (K. Schmidt-Rohr).

0032-3861/00/$ - see front matter © 2000 Elsevier Science Ltd. All rights reserved.
PII: S0032-3861(99)00429-2

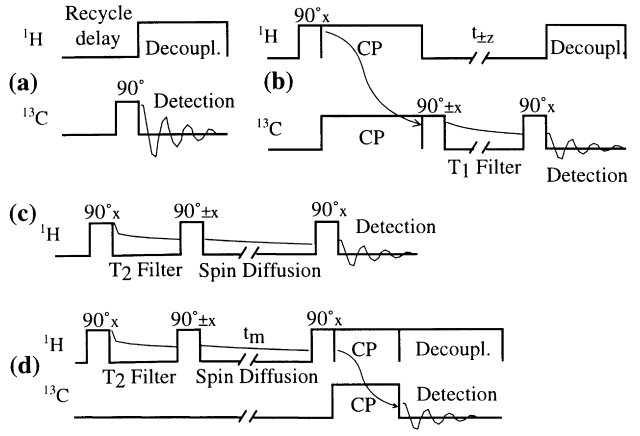

Fig. 1. Solid-state NMR pulse sequences used in this work. Except for minor modifications, they have been described in the literature. (a) Direct-polarization (DP) ^{13}C NMR experiment. (b) CP/$T_{1,C}$ experiment. Cross-polarization excites rigid regions efficiently. A $+z/-z$ phase cycle in alternate scans is introduced so that the final ($t_{\pm z} \rightarrow \infty$) signal is zero. (c) ^{1}H spin diffusion Goldman–Shen experiment (without sample rotation). (d) ^{1}H spin diffusion Goldman–Shen experiment with ^{13}C detection under magic-angle spinning.

segments are dispersed defects within the crystalline phase. This would lead to a structure very different from that of bulk HDPE material, where amorphous segments are aggregated and form extensive layers. To clarify this issue, it is necessary to determine the sizes of, and mobilities in, the crystalline and amorphous regions in the fibers. In the following, the domain sizes will be determined by ^{1}H spin diffusion and mobilities by ^{1}H and ^{13}C NMR spectra. Based on the NMR data and a comparison with other experimental facts, a structural model of UDF-PE will be proposed.

There are several other important morphological features of the fibers which have not been characterized conclusively. For example, based on NMR experiments, it has been claimed that a large (>25%) mobile but oriented interphase component is present in the fibers [16]. Also, it is not clear if there are any trapped entanglements (rigid *gauche* conformers) within the crystallites of ultradrawn PE. Finally, strong SAXS equatorial intensity (perpendicular to the fiber axis) in fibers with high draw ratio has been observed [5,17] and assigned to voids [17]. We will address these issues in this paper.

In addition to the intermediately mobile amorphous regions, a highly mobile fraction in drawn polyethylenes has been detected by ^{1}H wideline NMR [18,19]. But such a component was not observed in extruded PE by Porter and coworkers [20]. We will confirm the presence of a highly mobile phase in the drawn UDF-PE, which does not exist either in the extruded precursor material or after the fibers have been melted and re-crystallized. The size, chemical composition and physical origin of the highly mobile component will be discussed.

2. Experimental

A sample of ultradrawn UHMWPE fibers (cross-section 0.1×1.8 mm^2, referred to as UDF-PE in the following) was kindly provided by the late Prof. R.S. Porter. The molecular weight (viscosity average) is about 3×10^6. To produce the fibers, films of compacted Himont Hifax 1900 reactor powder were solid-state extruded at 110°C to a draw ratio of 5, followed by tensile drawing at 135°C. The final draw ratio achieved is 82–85, with tensile moduli of up to 130 GPa. No isotopic labeling was used. A commercial gel-spun UHMWPE fiber Spectra® 900 (gel-spun UDF-PE) was also studied for comparison.

The following samples were used in the various NMR experiments: (1) UDF-PE, placed in a 7 mm rotor for the MAS experiments, with the fiber axes along the rotor axis. (2) A uniaxially oriented UDF-PE sample for static NMR experiments: the fibers were aligned parallel to each other and wrapped with Teflon® tape. Two sections of 6 mm length were cut out and aligned parallel to each other in the NMR radio-frequency coil of 8 mm diameter. (3) Extruded UHMWPE (precursor of UDF-PE fiber) with extrusion ratio of 5 (E-PE). The dimensions of the sample are $5 \times 6 \times 15$ mm^3. (4) A bulk UHMWPE sample which was prepared by melting the UDF-PE fibers and cooling them in air (UDF-PE$_{melted}$). (5) Randomly oriented gel-spun UDF-PE fibers in a 7 mm rotor.

The dimensional density of UDF-PE and E-PE was determined by measuring the mass and the dimensions of the materials. The dimensions of E-PE were taken directly by a caliper. The width and length of UDF-PE were measured directly and the thickness was calculated by stacking many layers of the tapes together and measuring the total thickness. The dimensional density measured this way is 1.00 ± 0.03 g/cm^3 for E-PE, and 0.85 ± 0.03 g/cm^3 for UDF-PE, which agrees with the reduced dimensional density measured in highly drawn HDPE by Ward et al. [21].

The NMR experiments were performed on Bruker MSL 300 and DSX 300 spectrometers ($B_0 = 7$ T). Several different NMR pulse sequences were used in this study, as shown in Fig. 1: (1) Direct polarization (DP). ^{13}C magnetization is excited by a single 90° pulse (Fig. 1(a)). (2) A CP (cross polarization)/^{13}C T_1 ($T_{1,C}$) filter experiment [22] (Fig. 1(b)). The $T_{1,C}$ filter is created by storing the ^{13}C magnetization alternatively along the $\pm z$ direction after CP. The ^{13}C magnetization with shorter T_1 will survive the filter to a lesser extent. (3) Goldman–Shen experiment with ^{1}H detection using a dephasing time of 100 μs (Fig. 1(c)). The highly mobile phase was selected. (4) Goldman–Shen experiment with ^{13}C detection (Fig. 1(d)). The cross-polarization time was 1 ms. The dephasing time was 29.3 μs so that after the dephasing the crystalline signal vanishes but most of the amorphous signal is retained. In all experiments, the ^{1}H 90°-pulse lengths were 4.0 μs and the decoupling power was 80 kHz. The chemical shift calibration is based on a

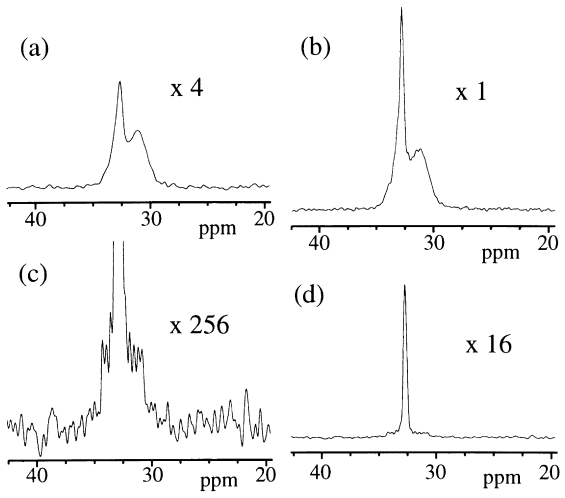

Fig. 2. ^{13}C direct-polarization spectra of UDF-PE demonstrating the procedure for crystallinity measurement. The spectra in (a)–(c) are rescaled to compensate for the different numbers of scans. (a) Recycle delay of 20 s, 512 scans. (b) Recycle delay of 50 s, 2048 scans. (c) Recycle delay of 10 000 s, 8 scans. (d) Same as (c), but scaled by 1/16 to show the crystalline peak fully. The small signal to the left of the peak of the predominant orthorhombic crystallites is due to the monoclinic crystal modification.

crystalline PE chemical shift of 32.8 ppm. One 90° pulse was used to obtain the ^1H signals, with a short dead-time delay of 3 μs before detection. The recycle delays used in the CP and proton experiments were 10 s. With such a recycle delay, the ^1H lineshape is the same as with an infinitely long recycle delay since during this period spin diffusion is efficient enough to equilibrate the magnetization.

3. Results

3.1. Crystallinity measurement

In the DP/MAS spectrum the amorphous and crystalline peaks appear at 31.3 and 32.8 ppm, respectively, as seen in Fig. 2(a) and (b). In order to calculate the crystallinity from the spectra, two problems have to be overcome: (1) Full relaxation of both components is required, but in UDF-PE the crystalline regions have an extremely long ^{13}C T_1 (~5000 s) (see Section 4). In addition, the amorphous component makes up only a small portion of the fibers. Therefore, the measurement time necessary to acquire a fully relaxed ^{13}C spectrum with good amorphous signal is intolerable (>10 days). (2) Crystalline and amorphous signals partially overlap.

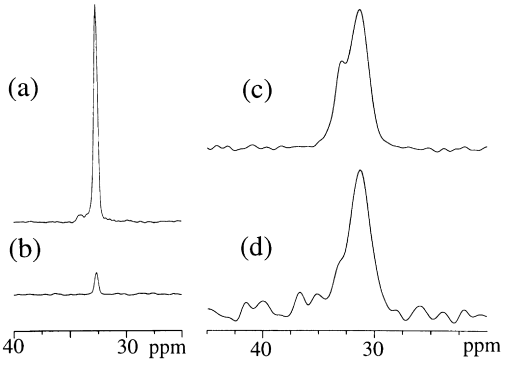

Fig. 3. (a) and (b): CP/$T_{1,C}$ filter spectra of UDF-PE with filter length of (a) 1 s and (b) 10 000 s. (c) and (d): Pure amorphous line shapes of UDF-PE obtained by (c) DP (recycle delay = 1 s) and (d) CP/$T_{2,H}$ filter (filter time = 16 μs).

The problems can be solved by a combination of four ^{13}C NMR experiments: (1) A DP experiment with a relatively short recycle delay and a large number of scans to measure the amorphous signal with good sensitivity. (2) A DP experiment with a long recycle delay and a small number of scans to measure the almost fully relaxed crystal signal. (3) A CP/$T_{1,C}$ filter experiment (Fig. 1) with the $T_{1,C}$-filter length equal to the recycle delay in experiment (2) to determine the correction factor for incomplete relaxation of the crystal signal. (4) An experiment to determine the pure amorphous signal line shape.

Since the amorphous regions have a short $T_{1,C}$, in experiment (1) we can observe the fully relaxed amorphous signal. To avoid the heteronuclear Overhauser enhancement of the ^{13}C signal, the recycle delay must be much longer than $T_{1,H}$. Recycle delays of 20 and 50 s were used, giving very similar amorphous signal heights per scan (Fig. 2(a) and (b)). However, in this spectrum the crystalline signal is incompletely relaxed. In experiment (2) where the recycle delay was long (10 000 s), a sufficiently strong crystalline signal is obtained but the amorphous signal is poor because of the low crystallinity and the small number of scans (Fig. 2(c) and (d)). So by combining two experiments (1) and (2), the relative intensity of the signals of the crystalline and amorphous regions can be obtained.

To determine the correction factor for incomplete relaxation after a recycle delay t_{RD} = 10 000 s, we performed the CP/$T_{1,C}$ filter experiment (3). Due to the phase cycling that stores the magnetization along $+z$ and $-z$ in alternate scans, the total intensity decays towards zero as a function of the $T_{1,C}$ filter time. The decay constant is the same as that in the signal increasing from zero towards the full equilibrium magnetization in the direct polarization experiment. The data in Fig. 3(a) and (b) show that at ambient temperature, the signal at t_{fil} = 10 000 s decays to 10% of the original signal, which was obtained with a short filter time of 1 s. This means that in the DP experiment with a recycle delay of 10 000 s the crystalline signal shows 90% of the fully relaxed intensity.

To separate out the amorphous component in the partially crystalline signal, we obtained pure amorphous line shapes in two different ways using (i) a DP/MAS experiment with very short recycle delay (1 s), and (ii) CP/$T_{2,H}$ filter experiment, where a free ^1H evolution (16 μs) before CP is applied and the crystalline-phase magnetization is destroyed as a result of the strong ^1H– ^1H dipolar couplings. The

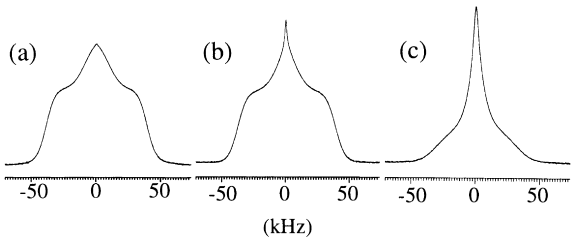

Fig. 4. ^{1}H wideline spectra of UHMWPE. (a) Extruded precursor, draw ratio $\lambda = 5$ (E-PE); (b) Ultradrawn fiber, draw ratio $\lambda = 82$–85 (UDF-PE). (c) Fiber material after melting and recrystallization (UDF-PE$_{melted}$). The ultradrawn fiber shows a narrow (i.e. highly mobile) component that is absent in the other spectra (for further proof see Fig. 6).

spectra are shown in Fig. 3(c) and (d). The area/height ratios for the two line shapes are equal within an error margin of 3%.

With the information obtained in the above experiments, the crystallinity can be calculated from the following formula:

$$f_{crystal} = \frac{A_c^{\infty}/NS_c}{\frac{A_c^{\infty}}{NS_c} + \frac{A_{ac}}{NS_{ac}}} = \frac{1}{1 + \frac{NS_c}{NS_{ac}}\frac{A_{ac}}{A_c^{\infty}}} \quad (1)$$

where A_c^{∞} is the area of the completely relaxed crystalline magnetization after NS_c scans, and A_{ac} is the fully relaxed amorphous component after a recycle delay of 20 or 50 s, with NS_{ac} scans.

The CP/T_1 correction leads to:

$$A_c^{\infty} = A_c/\left(1 - \frac{I_{cpfil}}{I_{cp}}\right) \quad (2)$$

where A_c is the area of crystalline signal at long recycle time (10 000 s), I_{cpfil} and I_{cp} are crystalline signal height in CP spectra with long (10 000 s) and short (1 s) $T_{1,C}$ filter, respectively.

From simple peak-shape considerations,

$$\frac{A_{ac}}{A_a} = \frac{I_{ac}}{I_a} \quad (3)$$

with the area A_a and height I_a of the pure amorphous line shape spectrum.

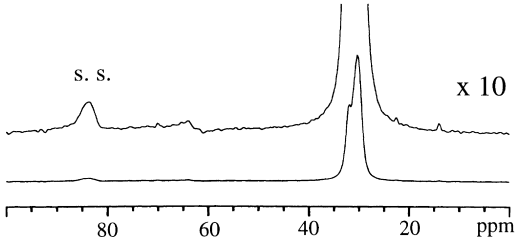

Fig. 5. ^{13}C direct polarization spectra of UDF-PE to detect impurities. The signal at 84 ppm is a spinning sideband (indicated by s.s.) of the major CH_2 peak. The dispersive signal at 63 ppm is background from outside the sample.

Thus, we obtain

$$f_{crystal} = \frac{1}{1 + \frac{NS_c}{NS_{ac}}\frac{A_a}{A_c}\frac{I_{ac}}{I_a}\left(1 - \frac{I_{cpfil}}{I_{cp}}\right)} \quad (4)$$

The ratio of the numbers of scans NS_c/NS_{ac} is exactly known. Thus, the crucial factor is the ratio of the pure amorphous and crystalline peak areas, each of which is available with good signal-to-noise ratio. The signal heights I_a and I_{ac} can be read off with high precision. Note that $(1 - I_{cpfil}/I_{cp})$ is a minor correction factor that deviates from unity typically by less than 10%.

The crystallinity result obtained based on Eq. (4) is (87.5 ± 1)%. Taking into account possible uncertainties from spectrometer instability which may lead to signal amplitude fluctuation, the crystallinity from our method is (88 ± 2)%. This value agrees with the ~90% crystallinity reported in the literature [5,8] based on density measurements for similar fibers with a draw ratio of ~100. It is higher than the simple DSC crystallinity of ~80% obtained for similar fibers [8]. Considering the uncertainties of the DSC method mentioned in the Section 1, we believe that our result is more reliable.

^{1}H spectra are often useful to obtain mobility information in materials. Fig. 4 shows the ^{1}H spectra of three samples: the extruded precursor (E-PE), the drawn fibers (UDF-PE), and the fiber material after melting (UDF-PE$_{melted}$). The chain axes of the first two samples were aligned along the magnetic field while the last sample is isotropic. In all the three spectra broad and narrow components are observed, associated with relatively rigid crystalline and mobile amorphous regions, respectively. The linewidth of the amorphous signal is narrower (i.e. the ^{1}H T_2 is longer) because the mobility of the segments in the amorphous regions partially averages out the strong ^{1}H– ^{1}H dipolar couplings. Based on the linewidth difference, the crystallinity of the fibers can be estimated from the ^{1}H spectrum. In Fig. 4(b), the crystalline and amorphous signals are quite clearly distinguished. In a wideline-separation experiment [23], the ^{1}H lineshape of the crystalline regions was determined. The crystallinity from the area ratio is (88 ± 2)%, which agrees very well with the ^{13}C NMR result. The ^{1}H result may be complicated by dead time and finite pulse-length problems; therefore, ^{13}C NMR is a more accurate way to determine the crystallinity in these materials.

3.2. A second, highly mobile amorphous phase in the fibers

In Fig. 4, the ^{1}H spectra of E-PE and UDF-PE$_{melted}$ show the typical two-phase feature of PE materials: a broad crystalline part and a narrower amorphous part. However, in the UDF-PE spectrum, besides these two phases, there is an additional sharper component with much higher mobility, as indicated by a ^{1}H line width of 1.8 ± 0.2 kHz. This highly mobile phase makes up (0.8 ± 0.2)% of the total sample.

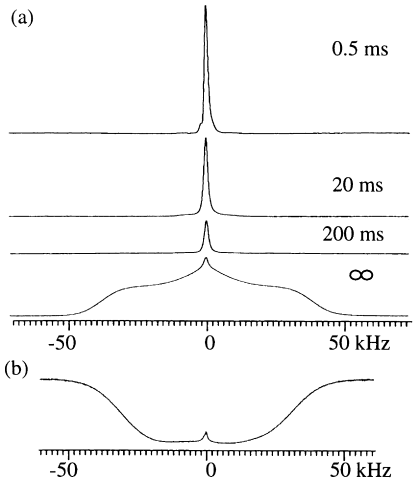

Fig. 6. (a) ^{1}H spin diffusion of UDF-PE from the highly mobile amorphous phase, after a $T_{2,H}$ filter of 100 μs duration with mixing times as indicated. At the bottom, the unfiltered spectrum (corresponding to infinite diffusion time) is shown for reference. Equilibrium is not achieved even after 200 ms of spin diffusion. (b) ^{1}H inversion recovery spectrum of UDF-PE, with a recovery time of 500 ms. The short $T_{1,H}$ and distinct nature of the highly mobile phase are apparent in its faster inversion recovery behavior.

The ^{1}H chemical shift of the component is 1.5 ± 0.1 ppm, which is the typical methylene proton value. To examine if it is a small-molecule impurity, a DP/MAS ^{13}C spectrum was measured with short recycle delay of 1 s, which is long enough for the $T_{1,C}$ relaxation of the highly mobile components (Fig. 5). From the chemical shift values, the small peaks at 14 and 23 ppm can be assigned to end groups (CH_3) and next-to-end CH_2 units. With the reasonable approximation that all the peaks in the spectrum are relaxed to the same extent and have a similar nuclear Overhauser enhancement, each small peak makes up 0.01% of the total ^{13}C signal (including crystalline). Assuming that the end groups are methyl groups and the chains are relatively free of long branches, these concentrations agree with those expected for end groups of polymers with a number-average molecular weight of ~300 000. If the highly mobile chains were short-chain paraffins, the end-group signal would be much higher. Therefore, the major component of the highly mobile phase must be polyethylene chains. A similar narrow ^{1}H signal was also found in the gel-spun Spectra® 900 fibers (gel-spun UDF-PE), with a similar concentration. Another mobile component which is separate from the highly mobile CH_2 units was found in this gel-spun material, with ^{13}C and ^{1}H chemical shifts of 4.0 and 71 ppm, respectively. It is assigned to ethylene oxide oligomers used as an additive to assist the gel-spinning process. Considering the different processing involved in the production of the two kinds of fibers, the presence of the highly mobile phase seems to be a universal feature of ultradrawn PE fibers.

Among the three spectral components, the narrow line of the highly mobile phase is least sensitive to dead time problems and other spectrometer limitations, and the isolated sharp line observed after ^{1}H T_2 selection (see Fig. 6) confirms its presence unequivocally. As regards the quantification, even if the area of the rigid components were underrepresented by 20% in Fig. 4, the fraction of highly mobile CH_2 groups would be reduced by only 0.2%, to 0.6%.

There is further strong evidence that this component is not a small-molecule impurity: (i) GPC of the fiber material shows no small MW products [24]. (ii) The UDF-PE fibers were produced by solid-state deformation, so no solvent was introduced; no other additives were put into the material either. (iii) The component is found neither in the precursor (E-PE) nor after recrystallization (UDF-PE_{melted}). A similar sharp component was also observed by other groups and ourselves in HDPE [18,19] that had been highly drawn without any use of additives (see Section 4).

To show that the small sharp signal indeed is due to very highly mobile segments and not just the narrowest part of the general amorphous signal, we selected it by a ^{1}H T_2 filter. By a very long $T_{2,H}$ filter time of 100 μs, the magnetization in both crystalline and normal amorphous regions were destroyed by dephasing and only that in the highly mobile phase survived (Fig. 6(a)) which was taken with a negligible spin diffusion time of 0.5 ms. This means that the highly mobile component has a much longer $T_{2,H}$ than the normal amorphous phase and the former is not a part of the latter, but a distinct phase. By contrast, in a $T_{2,H}$ dephasing experiment of UDF-PE_{melted}, all of the amorphous signal was uniformly suppressed by the filter. It was impossible to separate a component with longer $T_{2,H}$. This shows that the highly mobile component has vanished after melting and recrystallization.

A Goldman–Shen ^{1}H spin diffusion experiment was performed to obtain the information about the size of the highly mobile phase. First, a $T_{2,H}$ filter of 100 μs was applied to select the magnetization in the highly mobile phase while the magnetization in the crystalline and normal amorphous regions was destroyed by dephasing. Then the magnetization was flipped back to the z-direction and ^{1}H spin diffusion proceeded. Very little diffusion from the highly mobile phase to the other two phases was observed even after 200 ms of spin diffusion (Fig. 6(a)). Equilibrium was not achieved at very long diffusion time (>1 s) even if accelerated by the $T_{1,H}$ relaxation. In comparison, spin diffusion from >5 nm thick rubbery domains [25,26] or from 3 nm thick water layers between lipid bilayers [27] with even narrower protons lines proceeds much faster. Based on these references, the diameter of the highly mobile domains is estimated very conservatively as >3 nm. In fact, as discussed below, it is well possible that the highly mobile components do not form compact domains, but loose loops and isolated chains in voids of >100 nm diameter. Inversion recovery (Fig. 6(b)) shows that $T_{1,H}$ of the highly mobile component is less than 0.5 s, which is much shorter than for the other protons (>2 s for both amorphous and crystalline protons). This is further proof that the spin diffusion

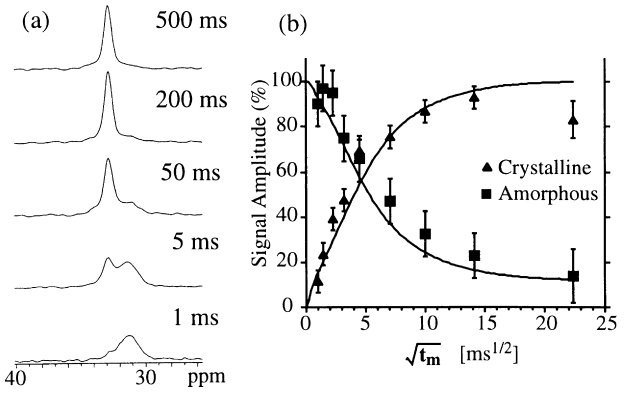

Fig. 7. ^{13}C-detected ^{1}H spin diffusion of UDF-PE from amorphous to crystalline regions. (a) Series of spectra with diffusion times of 1 to 500 ms as indicated. (b) Spin-diffusion plot of crystalline and amorphous signal intensities with fits. For fit parameters see text.

between the highly mobile components and the other regions is very slow.

3.3. Sizes of crystalline and amorphous regions

The crystalline and amorphous domain sizes can be characterized by ^{1}H spin diffusion [28,29]. The ^{1}H magnetization in the amorphous regions can be selected based on the longer ^{1}H T_2, and spin diffusion into the crystallites can be observed. A Goldman–Shen experiment with ^{13}C detection was performed to determine the domain sizes in the UDF-PE. The dephasing time was chosen so that the crystalline magnetization was exactly zero while the major part of the amorphous region magnetization was preserved. Equilibrium of magnetization across the two phases appears to be reached after 100 ms (Fig. 7). While the final value in the increasing crystalline-phase magnetization may be vaguely defined, the amorphous-phase magnetization will decrease to an asymptotic value of $1 - f_c$, where f_c is the crystallinity. The data show that this final value is nearly reached within the accessible mixing times.

A simulation based on a 1D spin diffusion model was performed (Fig. 7). The input information was: a crystallinity of 88% and lamellar morphology; spin diffusion coefficients in crystalline and amorphous regions of 0.8 and 0.15 nm^2/ms, respectively [30]. The data were corrected for T_1 relaxation to first order [28,29], but otherwise T_1 relaxation was not taken into account in the simulation. The best fit corresponds to an amorphous region size of 5.5 nm and crystallite diameter of 50 nm. These values should be understood as the smallest diameter rather than the average size of the domains. The true smallest thickness of the domains will be larger, since the fibers do not have a lamellar morphology. The simulation was based on a simple diffusion model appropriate for a lamellar morphology, where only one dimension (perpendicular to the lamellae) is relevant for the diffusion process. If more dimensions participate in the spin diffusion, e.g. two for cylindrical or three for spherical domains, the smallest domain size found from the initial slope in the spin diffusion plot increases proportional to this dimensionality [30]. Given that the amorphous regions are more likely to be dispersed in the crystalline matrix, a dimensionality of two is a reasonable estimate. The smallest diameter of the amorphous regions is thus estimated as 10 ± 5 nm, and the crystallite diameter as 100 ± 50 nm, with large error bars to account for the uncertainties in the shape and diffusion coefficient of the amorphous regions.

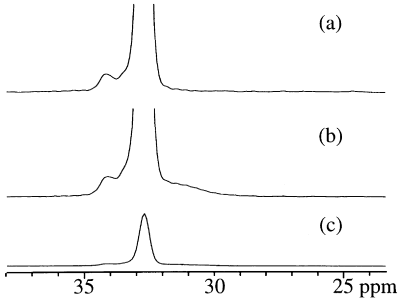

Fig. 8. CP and CP/$T_{1,C}$ filtered spectra of UDF-PE: (a) CP/$T_{1,C}$ filtered spectrum, filter length = 10 s selecting relatively immobile segments. No signal is observed in the 25 ~ 30 ppm range (*gauche* conformation). The signal at 34 ppm is from the monoclinic modification. (b) Regular CP spectrum for reference. The shoulder at 30 ~ 32 ppm is from the amorphous phase. (c) CP spectrum scaled by 1/10 to show the whole signal.

3.4. Search for immobile defects

In some models of the ultradrawn fibers, *gauche* conformers are considered to be embedded in the crystalline phase [11]. Based on the γ-*gauche* effect, ^{13}C NMR can distinguish between segments in all-*trans* conformation, which appear at >32.5 ppm, and in *gauche*-containing environments, with chemical shifts <32.5 ppm. Whereas the domain size of the amorphous phase detected above has shown that the majority of the *gauche* conformers form distinct amorphous regions instead of being dispersed in the crystalline phase, it is still interesting to investigate whether there are any dispersed "locked in" *gauche* defects. Rigid *gauche* segments would not undergo fast large amplitude motions (including *trans–gauche* or *gauche*$^+$/*gauche*$^-$ isomerizations); therefore, these segments should have a $T_{1,C}$ relaxation time comparable to that of the crystalline components. Since the rigid *gauche* segments should have both a long $T_{1,C}$ relaxation time and a high CP efficiency (comparable to that of the crystalline regions), a comparison of a simple CP and a CP/$T_{1,C}$ filter experiment can give information about the possible existence of these immobile defects. The spectra are shown in Fig. 8. In Fig. 8(b), the signals at 34 and 32.8 ppm are from the monoclinic [31,32] and the orthorhombic crystalline phase, respectively, with an area ratio of 1:23. The shoulder on the up-field side of the 32.8 ppm signal is from *gauche*-containing segments. In Fig. 8(a), the filter length was 10 s so that the mobile-amorphous components were screened out but the contribution of

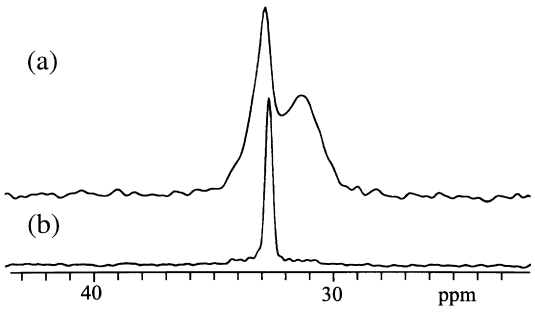

Fig. 9. ^{13}C direct-polarization spectra of UDF-PE at recycle delays of (a) 20 and (b) 10 000 s, respectively, taken from Fig. 2(a) and (d) to show the lineshape difference of the all-*trans* signals at different relaxation times. The fast relaxing signal in (a), which can be attributed to the crystalline–amorphous interface, has a significantly larger linewidth and slightly different chemical shift.

the rigid *gauche* segments would remain ($T_{1,C} \geq 10$ s). They would appear at the up-field side of the crystalline signal. In the spectrum of Fig. 8(a), no such *gauche* signal with long $T_{1,C}$ was found, which suggests that the rigid gauche component makes up less than 1% of the total rigid population.

4. Discussion

4.1. Sizes of crystalline and amorphous regions

At room temperature, the UDF-PE fiber has a long-time $T_{1,C}$ of 5000 s. The $T_{1,C}$ of crystalline PE has been studied with various samples and it was found that it depends mainly on the crystallite thickness [33]. If we assume that this conclusion can be extended to ultradrawn fibers, the $T_{1,C}$ of 5000 s corresponds to a crystal thickness of ~60 nm in UDF-PE [33]. This is in agreement with the result obtained by our spin diffusion experiment.

According to the domain size obtained from spin diffusion and the mobility of the amorphous regions reflected in the ^{13}H line shape, the amorphous regions are neither large separate pockets outside of huge continuous crystals, nor very small defects embedded in them. The size of the amorphous regions more likely resembles that in bulk HDPE.

Knowing the domain sizes, we are able to interpret the ^{1}H T_1 relaxation behavior. In the UDF-PE studied here, $T_{1,H}$ is about 3.2 s at room temperature, which is at least twice as long as in melt-crystallized high density polyethylenes. It increases slightly with temperature, to ~4.5 s at 360 K. Since the intrinsic $T_{1,H}$ in the crystalline regions expected on the basis of the ^{13}C T_1 is much longer, the measured $T_{1,H}$ values must reflect ^{1}H spin diffusion from the amorphous regions, where $T_{1,H}$ relaxation is relatively fast. Due to the high crystallinity, it takes the small amorphous fraction a longer time to relax the magnetization in the crystallites than it does in HDPE. The increase of $T_{1,H}$ in the crystallites with temperature reflects the increase of $T_{1,H}$ in the amorphous regions, which are in the fast-motion limit. There are two facts indicating that spin-diffusion is not the rate-limiting step: first, the Goldman–Shen experiment shows that equilibrium can be reached in 0.1 s, which is much shorter than $T_{1,H}$. Secondly, $T_{1,H}$ is mono-exponential to a good approximation.

4.2. A large interphase?

Recently, NMR data of ultradrawn PE fibers very similar to the UDF-PE investigated here were interpreted in terms of a 30% mobile and oriented interfacial fraction which has a ^{13}C T_1 of 1.8 s [16]. Our measurements show that this conclusion is incorrect. In the spectrum shown in Fig. 2(a), the interfacial fraction is nearly fully relaxed in the 20 s of recycle delay, yet makes up a much smaller area than the amorphous signal, which corresponds to about 10% of the total material. Actually, the same conclusion can be drawn from the first spectrum (with recycle delay of 10 s) in Fig. 2 of Ref. [7], which shows that the mobile oriented fraction is comparable to the amorphous fraction. Both observations show that the mobile and oriented interfacial fraction is less than 10%.

It is also important to note that the $T_{1,C}$ relaxation in the crystallites is mostly not due to an intrinsic mechanism but results from chain (or spin) diffusion from the amorphous regions [34–36]. So it has a $\sqrt{t}$ rather than an exponential time dependence. Therefore, the exponential fits to $T_{1,C}$ decay data to extract multiple components lack experimental support.

Still, the fast-relaxing crystalline component can be assigned to the interfacial regions, since the $T_{1,C}$ relaxation is mostly due to chain diffusion from the fast-relaxing amorphous regions [34–36]. ^{13}C direct-polarization spectra after recycle delays of 20 and 10 000 s (Fig. 9(a) and (b)) show that the fast-relaxing all-*trans* fraction has a distinctly larger ^{13}C MAS linewidth. Its full width at half maximum is 70 Hz, compared to 25 Hz for the crystalline core. The increased linewidth indicates that the segments near the interface have some limited mobility and disorder, while their chemical shift shows that they are still mostly all-*trans*. The all-*trans* signal after a recycle delay of 50 s (Fig. 2(b)) has a composite line shape which can be decomposed into 70- and 25-Hz components to a good approximation, indicating that a relatively clear boundary exists between the two components. In the total material, the fast relaxing, broadened all-*trans* component accounts for ~5%. In addition to the interface, taut-tie molecules [37,38] may also contribute to this signal.

4.3. The highly mobile phase

The series of spectra in Figs. 4 and 6 clearly show the presence of 0.8% of a highly mobile phase in UDF-PE, apparently induced by tensile drawing. A similar mobile fraction was also observed by other groups and ourselves in drawn high-density polyethylenes ($M_w \sim 10^5$) [18,19].

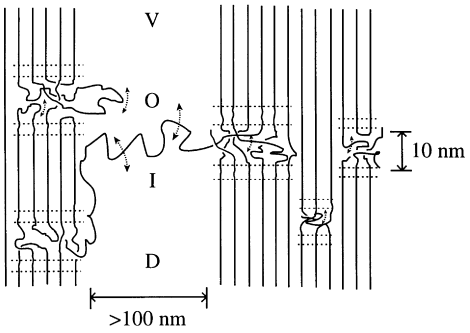

Fig. 10. Proposed phase structure of ultradrawn UHMWPE fibers, consisting of five components: 80% orthorhombic crystal, 3% monoclinic crystal, 5% crystal–amorphous interface (delineated by dashed lines), 11% amorphous region, and 0.8% highly mobile component. The monoclinic and orthorhombic crystallites are indicated by different spacings. The crystalline phase is continuous but the chains alternately traverse crystalline and amorphous regions. The interfacial segments are all-*trans* but have partial dynamical disorder. There are voids between the fibrils. The segments on the surface of the voids or traversing them are highly mobile (dashed arrows).

Smith et al. [18] and Kitamaru et al. [19] suggested that it was due to a low-molecular-weight fraction and to the segments which are close to the chain ends, respectively. However, there was no experimental proof for these arguments and it is not clear why these fractions should become observable only upon drawing.

By measuring the mass and dimension of the fibers, Ward et al. obtained a fiber density of ~0.8 g/cm^3, while by the floatation method, the density was close to 1.00 g/cm^3 [21]. They reasonably attributed this discrepancy to the existence of voids in the fibers. By SEM, they observed that the voids are long thin cavities between the fibrils, with widths greater than 100 nm [21]. The density of UDF-PE which we determined by measuring the mass and dimensions was (0.85 ± 0.03) g/cm^3, which is close to the result by Ward et al. In contrast, the density of the extruded precursor (E-PE) measured in the same way is (1.00 ± 0.03) g/cm^3. This suggests that the drawing process introduces a considerable volume of voids, while extrusion does not. An interesting fact is that the highly mobile phase was not observed in extruded PE (Fig. 6(a), also see Ref. [20]). These observations strongly suggest that voids may lead to the highly mobile phase.

A reasonable speculation to explain such a relationship is the following: the segments on the void surface and traversing the voids to connect different crystallites are highly mobile. Due to their mobility and limited contact with the crystallites and regular amorphous regions, spin diffusion from and to the highly mobile segments is slow. Since a material with many voids has a big surface area, the fibers will have a considerable amount of such a mobile component, as observed in the ^{1}H spectra. A rough estimate of the void size from the highly mobile fraction of 0.8%, the void volume fraction of 20%, and a hypothetical thickness of the mobile surface-layer component of 3 nm yields a diameter of ~300 nm, assuming the voids have a cylindrical shape. This is consistent with the widths of the voids observed by SEM [21].

Pennings and coworkers observed excess SAXS intensity in gel-spun PE fibers and ascribed it to the existence of voids [17]. Assuming that the voids are empty, they calculated a void volume fraction of 1% in hot-drawn gel-spun fibers. The discrepancy with the void volume fraction of ~15% obtained by the density measurements must be due to the fact that only the voids which are small enough (<100 nm) produce detectable SAXS intensity.

A highly mobile, liquid-like component on the surface of the fibrils will have properties of a lubricant. Indeed, it is well known that ultradrawn PE fibers have a very low friction coefficient and exceptionally good abrasion resistance compared, for instance, to carbon or Kevlar® fibers [1]. We suggest that this could be due to the highly mobile component on the surface of the PE fibrils.

4.4. A structural model for ultradrawn UHMWPE

The tensile modulus of ultradrawn PE fibers is close to the theoretical crystal modulus, which suggests that in the fibers there are continuous crystals along the fiber direction. In fact, long crystalline blocks (~3 μm) were found by transmission electron microscopy (TEM) [7]. On the other hand, our study shows that the material studied has a considerable mobile, *gauche*-containing amorphous component (~12%) with an average diameter of ~10 nm. A study of the same material has shown that the chain undergo 180° flips with rates of 1000/s at 360 K [39]. This mobility strongly suggests that most chains have alternate crystalline and amorphous portions. The fact that in hot drawing, a single molecule is drawn to a ratio significantly smaller than that of the whole material [40–42] and less than necessary for stretching the chain out completely [6,43] also requires that chains will have many folds which form amorphous regions. The seemingly contradictory observations of continuous crystals and small amorphous domains are accommodated by the following structural model for the ultradrawn polyethylene fibers: In every fibril the crystalline phase is continuous but an individual chain is not in a continuous crystal. The amorphous phase is dispersed in the crystal and most of the chains are alternately crystalline and amorphous. This is similar to the picture described in Ref. [44] where the high modulus is provided by the continuous crystalline phase, except that in our model there are few if any fully extended crystalline chains. The sizes of amorphous regions along a given chain are roughly comparable to those in melt-crystallized linear high-density polyethylene. There are voids between the fibrils and the segments on the surfaces are highly mobile. A schematic of this phase structure is shown in Fig. 10. Altogether, five morphological components have been identified: 83% crystal core, of which 80% is orthorhombic and 3% monoclinic, with a thickness of ~100 nm; 5% disordered all-*trans*

interfacial and/or tie molecules; 11% mobile amorphous regions, with diameters of ~10 nm; and 1% highly mobile segments, probably at void surfaces or traversing voids.

Acknowledgements

The authors would like to thank the late Prof R.S. Porter for providing the fibers and for many stimulating discussions. The work was funded by a Young Investigator Award from the Arnold and Mabel Beckman Foundation and by the National Science Foundation (grant DMR-9703916). Partial support was also provided by NSF/MRSEC.

References

[1] Lemstra PJ, Kirschbaum R, Ohta T, Yasuda H. In: Ward IM, editor. Developments in oriented polymers, vol. 2. London: Elsevier Applied Science, 1987. p. 1–39.
[2] Porter RS, Wang LH. J Macromol Sci—Rev Macromol Chem Phys C 1995;35:63.
[3] Smith P, Lemstra PJ. J Mater Sci 1980;15:505.
[4] Capaccio G, Ward IM. Nature Phys Sci 1973;243:143.
[5] Kanamoto T, Tsuruta A, Tanaka K, Takeda M, Porter RS. Macromolecules 1988;21:470.
[6] Hu WG, Schmidt-Rohr K. Acta Polym 1999, in press.
[7] Brady JM, Thomas EL. Polymer 1989;30:1615.
[8] Furuhata K, Yokokawa T, Seoul C, Miyasaka K. J Polym Sci: Polym Phys Ed 1986;24:59.
[9] Adams WW, Briber RM, Sherman ES, Porter RS, Thomas EL. Polymer 1985;26:17.
[10] Fischer EW, Goddar H. J Polym Sci: Pt C 1969;16:4405.
[11] Clark ES, Scott LS. Polym Engng Sci 1974;14:682.
[12] Peterlin A. Colloid Polym Sci 1975;253:809.
[13] Barham PJ, Arridge RGC. J Polym Sci: Polym Phys Ed 1977;15:1177.
[14] Arridge RGC, Barham PJ, Keller A. J Polym Sci: Polym Phys Ed 1977;15:389.
[15] Gibson AG, Davies GR, Ward IM. Polymer 1978;19:683.
[16] Chen W, Fu Y, Wunderlich B, Cheng J. J Polym Sci Part B: Polym Phys 1994;32:2661.
[17] Hoogsteen W, Brinke GT, Pennings AJ. J Mater Sci 1990;25:1551.
[18] Smith JB, Manuel AJ, Ward IM. Polymer 1975;16:57.
[19] Kitamaru R, Horii F. Adv Polym Sci 1978;26:137.
[20] Ito M, Kanamoto T, Tanaka K, Porter RS. Macromolecules 1981;14:1779.
[21] Smith JB, Davies GR, Capaccio G, Ward IM. J Polym Sci: Polym Phys Ed 1975;13:2331.
[22] Torchia DA. J Magn Reson 1978;30:613.
[23] Schmidt-Rohr K, Clauss J, Spiess HW. Macromolecules 1992;25:3273.
[24] Porter RS. Private discussions.
[25] Spiegel S, Schmidt-Rohr K, Boeffel C, Spiess HW. Polymer 1993;34:4566.
[26] Cai WZ, Schmidt-Rohr K, Egger N, Gerharz B, Spiess HW. Polymer 1993;32:267.
[27] Kumashiro KK, Schmidt-Rohr K, Murphy OJ, Ouellette KL, Cramer WA, Thompson LK. J Am Chem Soc 1998;120:5043.
[28] Packer KJ, Pope JM, Yeung RR, Cudby MEA. J Polym Sci: Polym Phys Ed 1984;22:589.
[29] Schmidt-Rohr K, Spiess HW. Multidimensional solid-state NMR and polymers. London: Academic Press, 1994.
[30] Clauss J, Schmidt-Rohr K, Spiess HW. Acta Polym 1993;44:1.
[31] VanderHart DL, Khoury F. Polymer 1984;25:1589.
[32] Tzou DL, Schmidt-Rohr K, Spiess HW. Polymer 1994;35:4728.
[33] Axelson DE, Mandelkern L, Popli R, Mathieu P. J Polym Sci: Polym Phys Ed 1983;21:2319.
[34] Schmidt-Rohr K, Spiess HW. Macromolecules 1991;24:5288.
[35] Robertson MB, Ward IM, Klein PG, Packer KJ. Macromolecules 1997;30:6893.
[36] Klein PG, Robertson MB, Driver MAN, Ward IM, Packer KJ. Polym Int 1998;47:76.
[37] Peterlin A. Polym Engng Sci 1978;18:488.
[38] Peterlin A. Colloid Polym Sci 1987;265:357.
[39] Hu WG, Boeffel C, Schmidt-Rohr K. Macromolecules 1999;32:1611.
[40] Sadler DM, Barham PJ. Polymer 1990;31:36.
[41] Sadler DM, Barham PJ. Polymer 1990;31:43.
[42] Sadler DM, Barham PJ. Polymer 1990;31:46.
[43] Kanamoto T, Porter RS. J Polym Sci: Polym Lett Ed 1983;21:1005.
[44] Taylor WN, Clark ES. Polym Engng Sci 1978;18:518.